

000 GTD: DYNAMIC GENERATION OF MULTI LLM 001 AGENTS COMMUNICATION TOPOLOGIES WITH GRAPH 002 DIFFUSION MODELS 003 004

006 **Anonymous authors**

007 Paper under double-blind review

011 ABSTRACT

013 The efficiency of multi-agent systems driven by large language models (LLMs)
014 largely hinges on their communication topology. However, designing an opti-
015 mal topology is a non-trivial challenge, as it requires balancing competing ob-
016 jectives such as task performance, communication cost, and robustness. Exis-
017 ting frameworks often rely on static or hand-crafted topologies, which inherently
018 fail to adapt to diverse task requirements, leading to either excessive token con-
019 sumption for simple problems or performance bottlenecks for complex ones. To
020 address this challenge, we introduce a novel generative framework called *Guided*
021 *Topology Diffusion (GTD)*. Inspired by conditional discrete graph diffusion mod-
022 els, GTD formulates topology synthesis as an iterative construction process. At
023 each step, the generation is steered by a lightweight proxy model that predicts
024 multi-objective rewards (e.g., accuracy, utility, cost), enabling real-time, gradient-
025 free optimization towards task-adaptive topologies. This iterative, guided synthe-
026 sis process distinguishes GTD from single-step generative frameworks, enabling
027 it to better navigate complex design trade-offs. We validated GTD across multi-
028 ple benchmarks, and experiments show that this framework can generate highly
029 task-adaptive, sparse, and efficient communication topologies, significantly out-
030 performing existing methods in LLM agent collaboration. Our code is available at
031 https://anonymous.4open.science/r/diffusion_agent-953C

032 1 INTRODUCTION

034 Large language model (LLM) driven multi-agent systems (MAS) increasingly rely on structured
035 communication to solve complex tasks, yet a core open problem is how to *dynamically* design the
036 communication topology for a given task and team. In practice, many systems still adopt hand-
037 crafted or heuristic patterns (e.g., chain, star, or fully connected graphs) or workflow templates and
038 role play frameworks (Wu et al., 2023; Hong et al., 2023; Li et al., 2023; Chen et al., 2023b). Such
039 static or rule-based designs struggle to adapt to the intrinsic complexity of the task, the composition
040 of skills required, or real-time progress. Classical MAS theory already shows that performance and
041 robustness depend critically on the underlying graph (e.g., consensus rates and failure modes are
042 tied to connectivity and spectral properties) (Zhu, 2006; Chen et al., 2013). The mismatch manifests
043 in practice: a simple Q&A may need only a short linear exchange, whereas software development
044 benefits from a richer collaboration network with project managers, programmers, and testers (Hong
045 et al., 2023). Using one pattern for all tasks either inflates token/communication overhead for sim-
046 ple problems or creates bottlenecks for complex ones (Zhang et al., 2024). Recent efforts begin to
047 *optimize* or *search* topologies, but typically emphasize end utility (accuracy) while underweighting
048 other crucial dimensions such as communication cost (token consumption), robustness to agent fail-
049 ures/attacks, and sparsity/efficiency (Zhang et al., 2025a; Sun et al., 2025; Zhou et al., 2025; Hu
050 et al., 2024b; Shang et al., 2024). Furthermore, their reliance on single-step generation mechanisms,
051 such as variational auto-encoders, can limit the fine-grained exploration of the multi-objective de-
052 sign space. A principled topology designer should therefore seek Pareto-optimal trade-offs in a
053 multi-objective space (Zhang et al., 2025c).

However, while these adaptive methods represent a significant step forward, they face two funda-
053 mental limitations. (1) First, their generative process often relies on single-step models like varia-

054
 055
 056
 057
 058
 059
 060
 061
 tional auto-encoders, which can struggle to capture the complex, long-range dependencies inherent in optimal communication structures. This may constrain the search space to topologies that are plausible but not truly Pareto-optimal. (2) Second, their optimization is often coarse-grained, applying reward signals only after a complete topology has been generated. Such post-hoc guidance makes it difficult to navigate the intricate trade-offs between competing objectives like task utility, token cost, and robustness in a fine-grained manner. The core research problem, therefore, is to develop a framework that can powerfully yet precisely construct topologies by integrating multi-objective guidance directly into each step of the generative process.

062
 063
 064
 065
 066
 067
 068
 069
 070
 071
 072
 073
 To address this challenge, we reframe topology synthesis as a guided, iterative construction process. We introduce **Guided Topology Diffusion (GTD)**, a framework that casts topology generation as a conditional discrete graph diffusion process, drawing on recent advances in generative modeling (Ho et al., 2020; Song & Ermon, 2021; Ho & Salimans, 2021; Vignac et al., 2023). By starting from a noisy graph and progressively denoising it, GTD leverages the strong generative capabilities of diffusion models to explore a richer design space. Crucially, we inject multi-objective guidance at each step of this reverse process. We achieve this by coupling the generator with a lightweight *proxy reward model* and performing *zeroth-order* (gradient-free) optimization during sampling, a scheme inspired by reward-modeling and gradient-free optimization practice (Nesterov & Spokoiny, 2017; Liu et al., 2018; Ouyang et al., 2022). This allows GTD to steer the generation trajectory in real-time, effectively balancing task utility, communication cost, and robustness to produce highly optimized, task-specific topologies.

074
 In summary, our contributions are threefold:

075
 076
 077
 078
 079
 080
 081
 082
 083
 084
 085
 086
 087
 088
 089
 090
 091
 092
 093
 094
 095
 096
 097
 098
 099
 100
 101
 102
 103
 104
 105
 106
 107
 ① **Problem Level:** We propose GTD, a novel conditional discrete graph diffusion framework for dynamically generating multi-agent communication topologies.

② **Algorithm Level:** We design and implement a proxy model-based zeroth-order optimization guidance algorithm, which effectively optimizes non-differentiable, high-cost external objectives during the diffusion process.

③ **Framework Level:** We construct a complete end-to-end solution that integrates advanced semantic feature encoding, conditional graph diffusion generation, and multidimensional protocol-based dynamic guidance, providing a new paradigm for solving such complex graph generation problems.

2 RELATED WORK

2.1 COMMUNICATION TOPOLOGIES IN MULTI-AGENT SYSTEMS

Classical MAS research establishes that communication topology strongly shapes global behavior: consensus speed and robustness depend on connectivity and spectral properties, while practical systems emphasize scalability and modularity over automatic topology synthesis (Zhu, 2006; 2003; Chen et al., 2013; Helsing et al., 2004; Ayal a, 2025). Analyses of star-like networks quantify the trade-off between rapid information propagation and single-point-of-failure risk (Chowdhury & Khalil, 2017; Gong et al., 2015). Learning within fixed or topology-constrained settings has been explored via cooperative RL (Xiao & Tan, 2013). Beyond LLM agents, multi-objective workflow schedulers and structural/topology optimization study Pareto

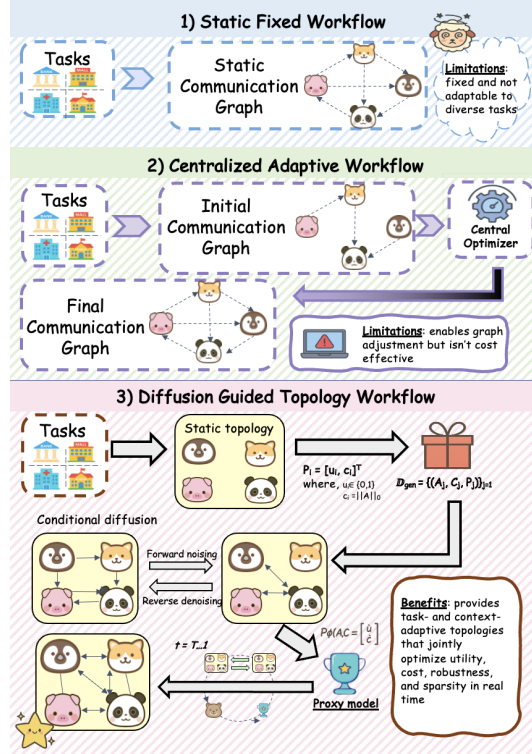


Figure 1: Comparison of Multi-Agent System (MAS) communication topology design workflows. (1) **Static Fixed Workflow**, (2) **Centralized Adaptive Workflow**, (3) **Diffusion Guided Topology Workflow (Ours)**. Our proposed method provides task- and context-adaptive topologies by using a conditional diffusion process guided by a proxy model to jointly optimize for utility, cost, robustness, and sparsity.

108 fronts (e.g., makespan, cost, reliability), motivating designs that jointly balance accuracy, sparsity,
 109 and resilience rather than optimizing a single metric (Zhang et al., 2025c; str, 2023).
 110

111 2.2 DYNAMIC TOPOLOGY GENERATION FOR LLM AGENTS 112

113 In LLM-based MAS, recent work reduces redundant exchanges and token budgets without changing
 114 the assumed graph class, or learns path-like collaboration schedules via next-agent prediction; others
 115 co-optimize prompts and wiring yet rely on task-agnostic heuristics (Zhang et al., 2024; Yang et al.,
 116 2025; Zhou et al., 2025). Closest to our setting are methods that *learn* the communication graph:
 117 G-Designer uses GNNs to design task-aware topologies (Zhang et al., 2025a), and Assemble-Your-
 118 Crew performs autoregressive graph generation conditioned on task context (Sun et al., 2025). Other
 119 approaches such as ExpoComm (Li et al., 2025), DACOM (Yuan et al., 2023), and MADRL (Zhu
 120 et al., 2025) address scalability and latency in decentralized settings.
 121

122 2.3 GRAPH DIFFUSION MODELS FOR SYNTHESIS 123

124 Recent advances in generative modeling have introduced powerful techniques for graph synthesis.
 125 Conditional graph diffusion models, in particular, have shown promise in various domains, inspir-
 126 ing our generative backbone (Xu et al., 2024; Vignac et al., 2023; Madeira et al., 2024). Our work
 127 also draws inspiration from other generative approaches for graphs like GCPN (You et al., 2018)
 128 and various communication-efficient paradigms (Lo et al., 2024; Du et al., 2024; Ding et al., 2024;
 129 Hu et al., 2024a; Zhao et al., 2024; Ji et al., 2025). Distinctly, our **GTD** is the first to integrate a
 130 fine-grained, proxy-guided zeroth-order optimization step directly into the sampling phase of a dis-
 131 crete graph diffusion process. This allows GTD to directly steer generation toward multi-objective
 132 optima (e.g. utility, token cost, sparsity, and robustness) without requiring differentiable or low-cost
 133 evaluators.
 134

135 3 PRELIMINARIES

136 In this section, we formalize the problem of topology generation and describe the underlying prin-
 137 ciples of graph diffusion models, pinpointing the limitations that motivate our proposed method.
 138

139 3.1 FORMALIZING TOPOLOGY GENERATION AS A CONDITIONAL GENERATIVE PROBLEM

140 The design of an optimal communication topology for a Multi-Agent System (MAS) can be framed
 141 as a conditional graph generation problem. Given a set of N agents, their communication structure
 142 is represented by a directed graph $G = (V, E)$, where $|V| = N$. This graph is fully described by its
 143 adjacency matrix $A \in \{0, 1\}^{N \times N}$, where $A_{ij} = 1$ signifies that agent i can send a message to agent
 144 j .
 145

146 **Optimization Objective.** For a given task query q and a set of available agents, which together
 147 form a task-specific condition vector C , the goal is to discover an optimal adjacency matrix A^* that
 148 maximizes a composite reward function $\mathcal{R}(A, C)$. This function evaluates the quality of a topology
 149 based on multiple criteria:
 150

$$152 \max_A \mathcal{R}(A, C) = f(\text{Utility}(A, C), \text{Cost}(A, C), \text{Sparsity}(A), \dots) \quad (1)$$

153 Here, **Utility** measures task success (e.g., accuracy), **Cost** quantifies token consumption or
 154 communication overhead, and **Sparsity** encourages efficiency. Evaluating $\mathcal{R}(A, C)$ is computa-
 155 tionally expensive, as it requires executing a full, costly multi-agent simulation for each candidate
 156 graph A .
 157

158 3.2 DENOISING DIFFUSION MODELS FOR GRAPH GENERATION

159 Denoising diffusion models are a class of powerful generative models that learn to synthesize data
 160 by reversing a gradual noising process. We adapt this paradigm for discrete graph structures.
 161

162 **Forward Diffusion Process.** The forward process, $q(A_t|A_0)$, systematically corrupts an initial
 163 graph A_0 by adding noise over T discrete timesteps. To operate in a continuous space, we first
 164 scale the adjacency matrix entries from $\{0, 1\}$ to $\{-1, 1\}$. The forward process is then defined as a
 165 variance-preserving schedule that adds Gaussian noise:

$$166 \quad q(A_t|A_0) = \mathcal{N}(A_t; \sqrt{\bar{\alpha}_t}A_0, (1 - \bar{\alpha}_t)I) \quad (2)$$

167 where $\{\beta_t\}_{t=1}^T$ is a predefined noise schedule, $\alpha_t = 1 - \beta_t$, and $\bar{\alpha}_t = \prod_{s=1}^t \alpha_s$. As $t \rightarrow T$, the
 168 distribution of A_T converges to a standard isotropic Gaussian distribution, $\mathcal{N}(0, I)$.
 169

170 **Learned Reverse Process.** The generative model learns the reverse process, $p_\theta(A_{t-1}|A_t, C)$, to
 171 denoise a noisy graph A_t and recover a cleaner version A_{t-1} , conditioned on the task context C .
 172 This is parameterized by a denoising network $\mathcal{G}_\theta(A_t, C, t)$, which is trained to predict the original
 173 clean graph A_0 from its noisy counterpart A_t . The training objective for \mathcal{G}_θ is to minimize the
 174 reconstruction error over a dataset of high-performing graphs:

$$175 \quad \mathcal{L}_\theta = \mathbb{E}_{t, A_0, C, \epsilon} \left[\|A_0 - \mathcal{G}_\theta(\sqrt{\bar{\alpha}_t}A_0 + \sqrt{1 - \bar{\alpha}_t}\epsilon, C, t)\|^2 \right] \quad (3)$$

177 where $\epsilon \sim \mathcal{N}(0, I)$. Once trained, we can generate a new graph by sampling $A_T \sim \mathcal{N}(0, I)$ and
 178 iteratively applying the denoising network to obtain A_0 .
 179

180 3.3 THE CHALLENGE: GUIDING GENERATION WITH A BLACK-BOX OBJECTIVE

181 A standard conditional diffusion model can generate topologies that are statistically similar to those
 182 in the training data, but it cannot explicitly optimize for the external reward function $\mathcal{R}(A, C)$ during
 183 generation. Steering the denoising process toward high-reward structures presents two major
 184 obstacles. First, the true reward function \mathcal{R} is too slow to be used for guidance within the iterative
 185 sampling loop, a challenge of **high-cost evaluation**. Second, the reward is a **non-differentiable**
 186 **“black-box” objective**; the output of the denoising network, \mathcal{G}_θ , is a continuous prediction that
 187 must be converted into a discrete graph A before evaluation, and this sampling step breaks the end-
 188 to-end differentiability, rendering gradient-based guidance techniques inapplicable. To overcome
 189 these challenges, we reframe the problem by introducing a method for efficient, gradient-free guid-
 190 ance. This is achieved by first training a lightweight **surrogate model (or proxy)** that accurately
 191 approximates the expensive reward \mathcal{R} and then using this proxy during inference to guide the diffu-
 192 sion sampling process with a **Zeroth-Order (ZO) optimization** scheme. This approach transforms
 193 the generation process from a simple denoising task into a guided synthesis, allowing us to directly
 194 optimize for task-specific, multi-objective rewards without requiring differentiability.
 195

196 4 METHODOLOGY

197 Our framework, **Guided Topology Diffusion (GTD)**, learns to generate optimal communication
 198 topologies for Multi-Agent System (MAS). GTD comprises two core components: (1) a **surrogate**
 199 **reward model**, \mathcal{P}_ϕ , that approximates the expensive simulation outcomes, and (2) a **conditional dif-
 200 fusion generator**, \mathcal{G}_θ , that learns the distribution of high-performing graph structures. We first train
 201 these components on a pre-computed dataset and then integrate them for a novel, guided synthesis
 202 process at inference time.
 203

204 4.1 SURROGATE REWARD MODEL

205 To circumvent the computational cost of direct simulation, we first train a surrogate model \mathcal{P}_ϕ to
 206 predict the performance of a given topology. This model maps a graph-condition pair (A, C) to a
 207 performance vector $[\hat{u}, \hat{c}]^T$, representing the predicted task utility and communication cost, respec-
 208 tively.
 209

210 **Architecture.** The surrogate \mathcal{P}_ϕ is implemented as a Graph Neural Network (GNN). Specifically,
 211 we employ a series of Graph Attention (GAT) layers to learn expressive node representations. The
 212 update rule for a node v ’s hidden state \mathbf{h}_v from layer (l) to $(l+1)$ is given by:
 213

$$214 \quad \mathbf{h}_v^{(l+1)} = \sigma \left(\sum_{u \in \mathcal{N}(v) \cup \{v\}} \alpha_{vu}^{(l)} \mathbf{W}^{(l)} \mathbf{h}_u^{(l)} \right) \quad (4)$$

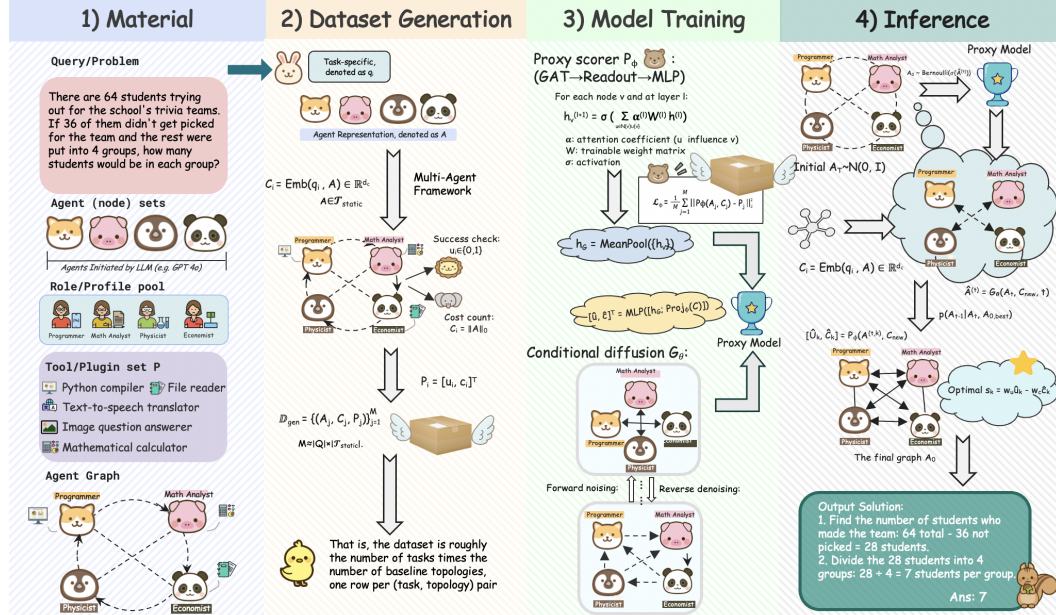


Figure 2: **The Guided Topology Diffusion (GTD) framework workflow**, divided into four main stages. **1) Material:** The process begins with task-specific inputs, including the query, available agents, and tools. **2) Dataset Generation:** A multi-agent framework simulates various baseline topologies to generate a foundational dataset linking topologies to performance outcomes (e.g., utility and cost). **3) Model Training:** The generated dataset is used to train two core components: a lightweight proxy scorer (P_ϕ) to predict topology performance and a conditional graph diffusion generator (G_θ) to learn the structure of high-performing graphs. **4) Inference:** For a new task, the framework uses the trained models to iteratively denoise a random graph, with the proxy scorer guiding each step to synthesize a final, task-optimized topology.

where $\alpha_{vu}^{(l)}$ are the learned attention coefficients between nodes v and u . The final node embeddings are aggregated via mean pooling to produce a graph-level representation \mathbf{h}_G . This is concatenated with the projected task condition vector C and processed by a multi-layer perceptron (MLP) to yield the final prediction: $[\hat{u}, \hat{c}]^T = \text{MLP}_\phi([\mathbf{h}_G; \text{Proj}_\phi(C)])$.

Training. We first generate a foundational dataset $\mathcal{D}_{\text{gen}} = \{(A_j, C_j, P_j)\}_{j=1}^M$ by running simulations for a diverse set of baseline topologies across various tasks. The model \mathcal{P}_ϕ is then trained to minimize the Mean Squared Error (MSE) loss between its predictions and the ground-truth performance vectors from simulation:

$$\mathcal{L}_\phi = \frac{1}{M} \sum_{j=1}^M \|\mathcal{P}_\phi(A_j, C_j) - P_j\|_2^2 \quad (5)$$

Model Fidelity. To ensure the surrogate provides effective guidance during the zeroth-order optimization step, we evaluated its performance on a held-out test split of the training dataset. The model achieves a low Mean Squared Error (MSE) for both utility and cost objectives, indicating it captures the underlying performance landscape accurately. Furthermore, we observed a strong positive correlation between the predicted and ground-truth cost metrics. Most importantly, when used to rank candidate graphs, the top-1 choice selected by the surrogate consistently coincides with the true best candidate in the majority of cases. These results confirm that \mathcal{P}_ϕ possesses sufficient ranking fidelity to steer the diffusion process toward Pareto-optimal regions.

4.2 CONDITIONAL GRAPH DIFFUSION GENERATOR

The core of our generative framework is a conditional diffusion model, \mathcal{G}_θ , designed to learn the distribution of high-quality topologies, $p_\theta(A|C)$. We explicitly chose Diffusion over single-shot approaches (e.g., VAEs or Gumbel-Softmax) to enable *iterative refinement*. In a discrete topology space, a single “wrong” edge can break the communication flow; diffusion allows our proxy model

270 to intervene at every step of the construction process, gently steering the graph toward high-reward
 271 regions gradually rather than risking mode collapse typical of one-shot generators.
 272

273 Here, in Figure 3, we provide a visual contrast between common static topologies and the sparse,
 274 adaptive structures that our generator is designed to create. This distinction highlights the frame-
 275 work’s goal: to move beyond one-size-fits-all patterns towards topologies optimized for the specific
 276 demands of a given task. We model the adjacency matrix $A \in \{0, 1\}^{N \times N}$ by scaling its values to
 277 $\{-1, 1\}$ and performing diffusion in a continuous space.
 278

279 **Diffusion Process.** We utilize a variance-preserving forward process $q(A_t | A_0)$ that gradually adds
 280 Gaussian noise to an initial graph A_0 over T timesteps:
 281

$$q(A_t | A_0) = \mathcal{N}(A_t; \sqrt{\bar{\alpha}_t} A_0, (1 - \bar{\alpha}_t) \mathbf{I}) \quad (6)$$

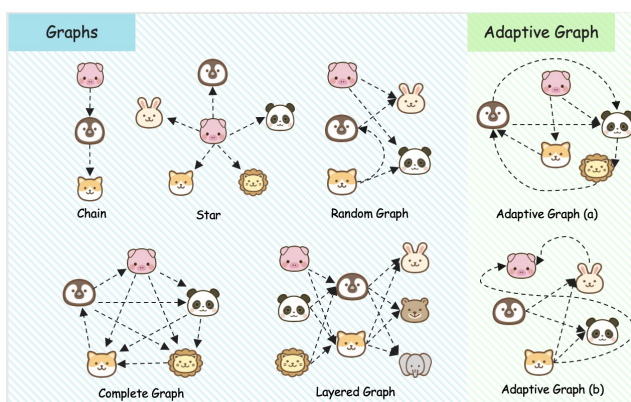
282 where $\{\beta_t\}_{t=1}^T$ is a fixed variance schedule and $\bar{\alpha}_t = \prod_{s=1}^t (1 - \beta_s)$. The objective is to learn the
 283 reverse process $p_\theta(A_{t-1} | A_t, C)$ to denoise a noisy graph A_t back towards a clean, high-performance
 284 graph, conditioned on the task vector C .
 285

286 **Denoising Network and Training.** We parameterize the reverse process with a denoising network
 287 $\mathcal{G}_\theta(A_t, C, t)$, which is implemented as a **Graph Transformer**. This architecture’s global attention
 288 mechanism is well-suited for capturing long-range dependencies inherent in graph topology opti-
 289 mization. **Critically, the Graph Transformer ensures that edges are not generated independently;**
 290 **the prediction of any single edge (i, j) is conditioned on the global context of all other nodes via**
 291 **self-attention, allowing the model to learn complex structural dependencies (e.g., cycles or hierar-**
 292 **chies).** The network is trained to predict the original graph A_0 from its noised version A_t . To focus
 293 the model on generating effective topologies, we train it exclusively on a high-performance subset
 294 $\mathcal{D}_{\text{hq}} \subset \mathcal{D}_{\text{gen}}$, where graphs exceed a certain performance threshold. The training objective is to
 295 minimize the binary cross-entropy (BCE) loss:
 296

$$\mathcal{L}_\theta = \mathbb{E}_{t, A_0 \sim p_{\text{hq}}, C, \epsilon} [\text{BCE}(\mathcal{G}_\theta(\sqrt{\bar{\alpha}_t} A_0 + \sqrt{1 - \bar{\alpha}_t} \epsilon, C, t), A_0)] \quad (7)$$

297 where $\epsilon \sim \mathcal{N}(0, \mathbf{I})$. This objective serves as a practical surrogate for maximizing the true Evidence
 298 Lower Bound, a connection we formalize in Appendix C (see Theorem C.3).
 299

300 4.3 PROXY-GUIDED TOPOLOGY SYNTHESIS



316 **Figure 3: An illustration of different multi-agent communication topologies.** The left panel shows examples of common static
 317 or heuristic graphs, such as **Chain**, **Star**, **Complete**, **Layered**, and **Random** graphs.
 318 The right panel shows examples of **Adaptive Graphs**, which represent the sparse, task-specific topologies that
 319 the GTD framework is designed to generate dynamically.
 320

321 322 323 timestep t , we first use the generator \mathcal{G}_{θ^*} to predict the unguided clean graph, $\hat{A}_0^{(t)}$. We then sample

324 At inference, we synthesize a topology for a novel task condition C_{new} by steering the diffusion process with
 325 the trained surrogate model \mathcal{P}_{ϕ^*} . The condition vector C is formed by concatenating the semantic embedding
 326 of the task query q (obtained via a pre-trained encoder) with the current graph state embeddings. This ensures
 327 the guidance is context-aware.
 328

329 Standard guidance techniques (e.g., classifier-free guidance) require gradients from the guiding model. How-
 330 ever, our surrogate \mathcal{P}_{ϕ^*} evaluates discrete graph samples, making its out-
 331 put non-differentiable with respect to the generator’s continuous predictions.
 332

333 To overcome this, we introduce a **zero-order (ZO) optimization** step within each denoising iteration. As
 334 detailed in Algorithm 1, at each

Method	GSM8K	MATH	MultiArith	HumanEval	MMLU	SVAMP	Avg.
Vanilla	87.45	46.29	96.85	87.08	82.14	86.67	81.75
CoT	87.10 $\downarrow 0.35$	46.40 $\uparrow 0.11$	96.31 $\downarrow 0.54$	88.13 $\uparrow 1.05$	82.65 $\uparrow 0.51$	87.33 $\uparrow 0.66$	81.99 $\uparrow 0.24$
ComplexCoT	86.89 $\downarrow 0.56$	46.53 $\uparrow 0.24$	96.70 $\downarrow 0.15$	87.49 $\uparrow 0.41$	83.78 $\uparrow 1.64$	87.67 $\uparrow 1.00$	81.84 $\uparrow 0.09$
SC (CoT \times 5)	87.57 $\uparrow 0.12$	47.91 $\uparrow 1.62$	96.58 $\downarrow 0.27$	88.60 $\uparrow 1.52$	82.66 $\uparrow 0.52$	88.00 $\uparrow 1.33$	81.89 $\uparrow 0.14$
MultiPersona	87.50 $\uparrow 0.05$	45.43 $\downarrow 0.86$	97.49 $\uparrow 0.64$	88.32 $\uparrow 1.24$	83.65 $\uparrow 1.51$	87.00 $\uparrow 0.33$	81.90 $\uparrow 0.15$
LLM-Debate	89.47 $\uparrow 2.02$	48.54 $\uparrow 2.25$	97.33 $\uparrow 0.48$	88.68 $\uparrow 1.60$	83.69 $\uparrow 1.55$	89.00 $\uparrow 2.33$	82.79 $\uparrow 1.04$
LLM-Blender	88.35 $\uparrow 0.90$	46.92 $\uparrow 0.63$	97.29 $\uparrow 0.44$	88.80 $\uparrow 1.72$	81.22 $\downarrow 0.92$	87.33 $\uparrow 0.66$	81.65 $\downarrow 0.10$
DyLAN	89.98 $\uparrow 2.53$	48.63 $\uparrow 2.34$	97.12 $\uparrow 0.27$	90.42 $\uparrow 3.34$	80.16 $\downarrow 1.98$	88.67 $\uparrow 2.00$	82.50 $\uparrow 0.75$
AgentVerse	89.91 $\uparrow 2.46$	47.35 $\uparrow 1.06$	97.50 $\uparrow 0.65$	89.29 $\uparrow 2.21$	81.22 $\downarrow 0.92$	88.33 $\uparrow 1.66$	82.27 $\uparrow 0.52$
MacNet	87.95 $\uparrow 0.50$	45.18 $\downarrow 1.11$	96.03 $\downarrow 0.82$	84.57 $\downarrow 2.51$	79.85 $\downarrow 2.29$	86.00 $\downarrow 0.67$	79.93 $\downarrow 1.82$
AutoAgents	87.69 $\uparrow 0.24$	45.32 $\downarrow 0.97$	96.42 $\downarrow 0.43$	87.64 $\uparrow 0.56$	82.13 $\downarrow 0.01$	86.34 $\downarrow 0.33$	80.96 $\downarrow 0.79$
GPTSwarm	89.14 $\uparrow 1.69$	47.88 $\uparrow 1.59$	96.79 $\downarrow 0.06$	89.32 $\uparrow 2.24$	83.98 $\uparrow 1.84$	88.67 $\uparrow 2.00$	82.96 $\uparrow 1.21$
ADAS	86.12 $\downarrow 1.33$	43.18 $\downarrow 3.11$	96.02 $\downarrow 0.83$	84.19 $\downarrow 2.89$	77.93 $\downarrow 4.21$	86.33 $\downarrow 0.34$	78.96 $\downarrow 2.79$
AgentSquare	87.62 $\uparrow 0.17$	48.51 $\uparrow 2.22$	97.77 $\uparrow 0.92$	89.08 $\uparrow 2.00$	79.85 $\downarrow 2.29$	88.00 $\uparrow 1.33$	81.81 $\uparrow 0.06$
AFlow	91.16 $\uparrow 3.71$	51.28 $\uparrow 4.99$	96.22 $\downarrow 0.63$	90.93 $\uparrow 3.85$	83.28 $\uparrow 1.14$	88.33 $\uparrow 1.66$	83.53 $\uparrow 1.78$
G-Designer	92.09 $\uparrow 4.64$	51.00 $\uparrow 4.71$	97.78 $\uparrow 0.93$	91.11 $\uparrow 4.03$	84.50 $\uparrow 2.36$	90.00 $\uparrow 3.33$	84.41 $\uparrow 2.66$
MaAS	92.30 $\uparrow 4.85$	51.82 $\uparrow 5.53$	98.80 $\uparrow 1.95$	90.56 $\uparrow 3.48$	83.78 $\uparrow 1.64$	89.67 $\uparrow 3.00$	84.49 $\uparrow 2.74$
GTD (Ours)	94.14 $\uparrow 6.69$	54.07 $\uparrow 7.78$	98.88 $\uparrow 2.03$	91.46 $\uparrow 4.38$	84.58 $\uparrow 2.44$	91.33 $\uparrow 4.66$	85.74 $\uparrow 3.99$

Table 1: Performance comparison on various benchmarks. All scores are accuracy (%). Changes are reported relative to the **Vanilla** baseline. The **best result** in each column is bolded. Baselines: CoT (Wei et al., 2022), ComplexCoT (Fu et al., 2022), SC (CoT \times 5) (Wang et al., 2023a), MultiPersona (Wang et al., 2023b), LLM-Debate (Du et al., 2023), LLM-Blender (Jiang et al., 2023), DyLAN (Liu et al., 2023), AgentVerse (Chen et al., 2023b), MacNet (Qian et al., 2024), AutoAgents (Chen et al., 2023a), GPTSwarm (Zhuge et al., 2024), ADAS (Hu et al., 2024b), AgentSquare (Shang et al., 2024), AFlow (Zhang et al., 2025d), G-Designer (Zhang et al., 2025a) MaAS (Zhang et al., 2025b).

K discrete candidate graphs from this prediction. The surrogate model \mathcal{P}_{ϕ^*} evaluates all candidates, and we select the one that maximizes our composite reward objective:

$$A_{0,\text{best}}^{(t)} = \arg \max_{A_{0,k}^{(t)}} (w_u \cdot \hat{u}_k - w_c \cdot \hat{c}_k) \quad \text{s.t.} \quad [\hat{u}_k, \hat{c}_k]^T = \mathcal{P}_{\phi^*}(A_{0,k}^{(t)}, C_{\text{new}}) \quad (8)$$

This best-ranked candidate, $A_{0,\text{best}}^{(t)}$, is then used in place of the original prediction $\hat{A}_0^{(t)}$ to compute the posterior distribution $q(A_{t-1}|A_t, A_{0,\text{best}}^{(t)})$ for sampling the next state A_{t-1} . **By shifting the mean of the posterior distribution toward $A_{0,\text{best}}^{(t)}$, we effectively bias the sampling trajectory toward high-reward regions without requiring gradients.** This procedure directly injects task-specific performance objectives into the generative trajectory.

$$A_{0,\text{best}}^{(t)} = \arg \max_{A_{0,k}^{(t)}} (w_u \cdot \hat{u}_k - w_c \cdot \hat{c}_k) \quad \text{s.t.} \quad [\hat{u}_k, \hat{c}_k]^T = \mathcal{P}_{\phi^*}(A_{0,k}^{(t)}, C_{\text{new}}) \quad (9)$$

This best-ranked candidate, $A_{0,\text{best}}^{(t)}$, is then used in place of the original prediction $\hat{A}_0^{(t)}$ to compute the posterior distribution $q(A_{t-1}|A_t, A_{0,\text{best}}^{(t)})$ for sampling the next state A_{t-1} . This procedure directly injects task-specific performance objectives into the generative trajectory, guiding the synthesis towards topologies that are optimized for the given task. The effectiveness of this guidance is directly tied to the fidelity of the surrogate model \mathcal{P}_{ϕ^*} . In Appendix C, we formally bound the performance gap of the resulting topology as a function of the surrogate’s approximation error (Theorem C.5).

378

5 EXPERIMENTS

380 To validate the effectiveness of our proposed **GTD** framework, we conduct a comprehensive set
 381 of experiments designed to evaluate its performance across three key dimensions: **(1) task-solving**
 382 **effectiveness**, **(2) communication cost-efficiency**, and **(3) robustness against agent failures**.
 383

384 Our experimental setup is standardized across all evaluations to enable fair comparisons. The back-
 385 bone for all agents is **GPT-4o-mini**. In our primary experiments, we deploy domain-specific agent
 386 teams: four **MathSolver** agents for the mathematics datasets (GSM8K, MATH, MultiArith, and
 387 SVAMP); four **CodeSolver** agents for the coding dataset (HumanEval); and three **Knowledge-
 388 ableAcademic** agents for the science dataset (MMLU). The surrogate reward model (\mathcal{P}_ϕ) in the
 389 **GTD** framework is a Graph Neural Network with two GAT layers and a hidden dimension of 32,
 390 trained for 10 epochs using the Adam optimizer with a learning rate of 1e-3 and a batch size of 16
 391 to minimize mean squared error loss. The conditional diffusion generator (\mathcal{G}_θ) is a two-layer Graph
 392 Transformer with two attention heads optimized with a learning rate of 1e-4, and the diffusion pro-
 393 cess runs for 50 timesteps. To demonstrate data efficiency, the training dataset for these models was
 394 constructed by evaluating baseline topologies on datasets. During inference, proxy-guided synthesis
 395 applies a zeroth-order optimization step, evaluating five candidate graphs ($K = 5$) at each timestep
 396 to guide the generation process using an inference batch size of 2. The training dataset was con-
 397 structed by evaluating baseline topologies on a minimal subset of only 50 samples from the training
 398 set. Using GSM8K as an example, this approach demonstrates high data efficiency, as the initializa-
 399 tion overhead is negligible; the one-time token cost for generating training data ($\approx 4.0 \times 10^5$ tokens)
 400 is rapidly amortized by the millions of tokens saved during inference on the full test set ($\approx 4.4 \times 10^6$
 401 tokens per run), resulting in significant net efficiency gains for the system.

402 During inference, proxy-guided synthesis applies a zeroth-order optimization step, evaluating five
 403 candidate graphs at each timestep to guide the generation process.

404

5.1 TASK-SOLVING EFFECTIVENESS

405 First, we evaluated GTD’s ability to generate high-utility communication topologies by comparing
 406 its task-solving performance against a wide range of established multi-agent methods. We used
 407 several popular benchmarks for this comparison, including GSM8K, MATH, MultiArith for math-
 408 ematical reasoning, and HumanEval for code generation. Baselines include canonical prompting
 409 strategies like Chain-of-Thought (CoT) (Wei et al., 2022) as well as more recent agentic frame-
 410 works such as AgentVerse (Chen et al., 2023b), AFlow (Zhang et al., 2025d), and MaAS (Zhang
 411 et al., 2025b). For each task, GTD generates a bespoke communication topology conditioned on the
 412 problem description, and the resulting multi-agent system solves the task. Performance is measured
 413 by task-specific accuracy.

414 As shown in Table 1, GTD demonstrates superior performance across the majority of benchmarks.
 415 It achieves state-of-the-art results on GSM8K (94.14), MATH (54.07), MultiArith (98.88), and
 416 SVAMP (91.30), significantly outperforming all baselines. For instance, on the challenging MATH
 417 dataset, GTD improves upon the strongest baseline (MaAS) by over 2 absolute percentage points.
 418 This highlights our framework’s ability to generate highly effective, task-adaptive topologies that
 419 facilitate better collaboration among agents compared to static or heuristically-designed commu-
 420 nication structures. **To ensure our findings are robust across different model families and task**
 421 **complexities, we also validated GTD on open-source models (Qwen-3-8B) and harder benchmarks**
 422 **(LiveCodeBench). Please refer to Appendix E for these additional results. These supplementary**
 423 **experiments confirm that GTD’s topological optimization transfers effectively to diverse backbones**
 424 **and modern coding challenges, reinforcing the method’s broad applicability beyond standard rea-**
 425 **soning tasks.**

426

5.2 COMMUNICATION COST-EFFICIENCY

427 A core motivation for dynamic topology generation is to reduce unnecessary communication and
 428 minimize token consumption. Our analysis confirms that GTD generates not only effective but also
 429 significantly sparser and more cost-efficient topologies compared to methods that rely on dense or
 430 fully-connected graphs.

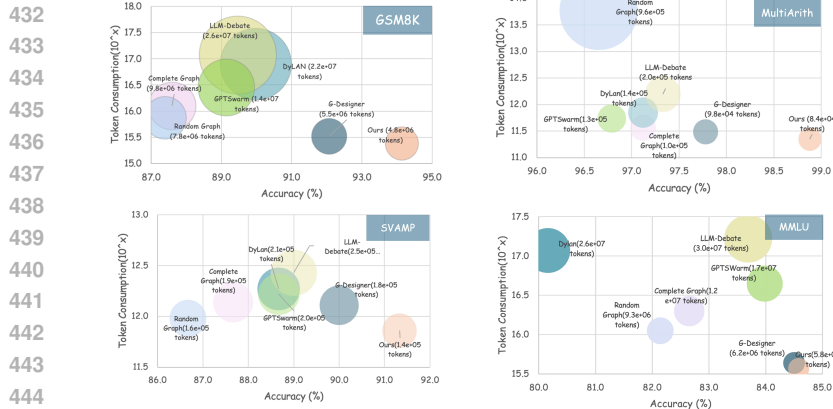


Figure 4: Accuracy versus token consumption for various multi-agent methods across the GSM8K, MultiArith, MMLU, and SVAMP benchmarks. The plots illustrate that topologies generated by GTD are highly cost-efficient, achieving strong performance while using significantly fewer tokens than baseline methods that rely on dense communication graphs.

accuracy, while methods like LLM-Debate use over five times the tokens. This efficiency is even more pronounced on MultiArith, where GTD reaches nearly 99% accuracy using just 8.4e+04 tokens, setting a new Pareto frontier that no other method approaches. Similarly, on SVAMP, GTD is the only method to surpass 91% accuracy while keeping token usage at a minimum (1.4e+05 tokens). These findings show that the proxy-guided generation process successfully learns to create sparse, efficient graphs by preserving only the most critical communication links, thereby avoiding the quadratic overhead of fully-connected approaches while still enabling complex, high-performance interactions. Crucially, this massive reduction in operational token cost ensures that the one-time setup cost for training the proxy is rapidly amortized, granting GTD a net efficiency advantage over zero-shot baselines immediately upon deployment.

5.3 ROBUSTNESS AGAINST AGENT FAILURES

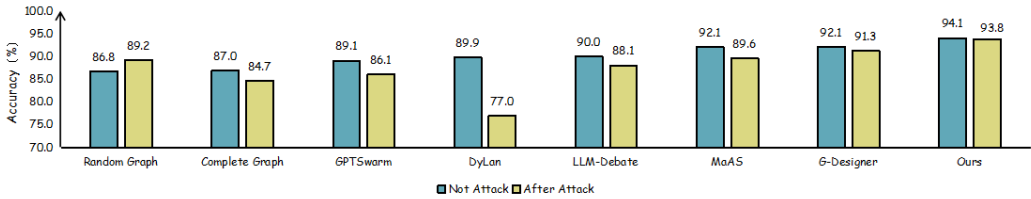


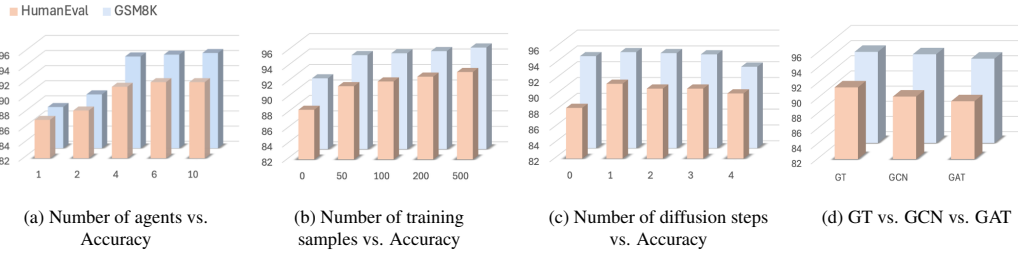
Figure 5: Robustness of various multi-agent systems to simulated agent failure on the GSM8K benchmark. The chart compares task accuracy before and after an attack, demonstrating that topologies generated by GTD exhibit greater resilience and more graceful performance degradation compared to other methods.

The structure of a communication graph critically impacts a multi-agent system’s resilience. To evaluate this, we tested the robustness of GTD-generated topologies by simulating agent failures during task execution on the GSM8K benchmark. In the experiment, a non-critical agent was randomly selected and its failure was simulated by making it produce erroneous outputs.

The results in the Figure 9 above demonstrate that GTD-generated topologies are significantly more robust to agent failure than those from all other compared methods.

While all systems experienced some performance degradation, GTD’s accuracy dropped by a mere 0.3 percentage points (from 94.1% to 93.8%), showcasing a remarkably graceful degradation. This stands in stark contrast to other methods; for instance, DyLan’s accuracy plummeted by nearly 13 points, and even a Complete Graph topology dropped by over 2 points. This experiment confirms that by jointly optimizing for multiple objectives, GTD learns to generate topologies with sufficient redundancy to bypass failed agents, ensuring high resilience in practical, imperfect scenarios.

The results, visualized in the scatter plots in Figure 4, show GTD’s exceptional efficiency. Across all tested benchmarks: GSM8K, MultiArith, SVAMP, and MMLU, GTD consistently occupies the optimal bottom-right position, signifying the highest accuracy achieved with the lowest token consumption. For instance, on GSM8K, GTD achieves over 94% accuracy while consuming only 4.8e+06 tokens; in contrast, the next best performer, G-Designer, requires 15% more tokens for lower accuracy.

486
487
488
489
6 ABLATION STUDIES
490
491
492
493
494

495
496
497
Figure 6: **Ablation studies on key hyperparameters and components of the GTD framework.** From left
498 to right, the charts show the framework’s sensitivity to: (1) the number of agents, (2) the number of training
499 samples, (3) the number of diffusion steps, and (4) the choice of denoising network architecture. The results
500 consistently validate our primary design choices.

Variant	GSM8K	HumanEval
GTD (Ours)	94.14	91.43
– w/o Guidance	88.42	87.19
– w/ Random	89.65	88.32

501
502
503
504
505
506
507
508
Figure 7: Ablation study on the impact of the
509 proxy guidance mechanism.

511
512 intelligent selection offered only a minor improvement,
513 key driver of success.

514
515 Our analysis of agent team size, visualized in Figure 6 (left), revealed that performance scales ef-
516 fectively up to four agents but shows diminishing returns thereafter. This result validates our use
517 of four agents as an optimal trade-off between task performance and computational efficiency. We
518 also found the framework to be highly data-efficient, with the largest performance gains achieved
519 within the first 50 training samples (Figure 6, second from left). This demonstrates that GTD can
520 be trained effectively without requiring a massive, expensive dataset. Furthermore, while current
521 reasoning benchmarks saturate at smaller team sizes, our framework is technically capable of scal-
522 ing to significantly larger agent populations without hitting memory bottlenecks (see Appendix D),
523 ensuring its applicability to more complex future scenarios.

524
7 CONCLUSION
525

526
527 Existing Multi-Agent Systems (MAS) often rely on static, hand-crafted topologies that do not adapt
528 to diverse tasks, leading to either excessive token consumption for simple problems or performance
529 bottlenecks for complex ones. To address this, we introduce Guided Topology Diffusion (GTD), a
530 novel generative framework that uses conditional discrete graph diffusion models to iteratively con-
531 struct a communication network. Experiments show that GTD creates highly task-adaptive, sparse,
532 and efficient topologies that significantly outperform existing methods in LLM agent collaboration
533 and demonstrate superior robustness to agent failures. However, a limitation remains in the depen-
534 dency on the initial seed dataset for training the proxy, which, despite being small, requires domain-
535 specific simulation data. As for future work, we will explore online active learning mechanisms to
536 update the proxy in real-time, eliminating the offline warm-up phase entirely. Additionally, we plan
537 to extend GTD to support dynamic, time-varying topologies that evolve continuously throughout the
538 multi-agent conversation, rather than being fixed at the start.

539
To rigorously validate our design choices, we
conducted a series of ablation studies to iso-
540 late the contribution of GTD’s core components
and hyperparameters, with results summarized
541 in Figure 6 and Figure 7. The most critical find-
542 ing, shown in Figure 7, confirms the impact of
543 our proxy-guided synthesis; removing the guid-
544 ance mechanism entirely causes a performance
545 drop of nearly 6 percentage points on GSM8K
(from 94.14% to 88.42%). Furthermore, using
546 random guidance instead of the proxy model’s
547

540
541
ETHICS STATEMENT

542 Our work aims to improve the efficiency of multi-agent systems (MAS), which can reduce computational costs and accelerate progress in beneficial domains. We acknowledge, however, that the
 543 underlying training process require computing resources and that any powerful coordination framework
 544 could be potentially misused for malicious ends. The performance of our method also depends
 545 on the initial training data, which could introduce biases if not carefully curated. We therefore ad-
 546 vocate for the responsible development of agentic AI and encourage further research into the safety,
 547 fairness, and transparency of dynamically structured MAS to mitigate these risks.
 548

549
550
REPRODUCIBILITY STATEMENT
551

552 To ensure the reproducibility of our research, this paper provides a detailed account of our method-
 553 ology and experimental setup. The core components of our Guided Topology Diffusion (GTD)
 554 framework, including the surrogate reward model and conditional diffusion generator, are described
 555 in Section 4, with the generation process detailed in Algorithm 1. Our complete experimental proto-
 556 col, including the LLM backbone, benchmarks, and agent configurations, is presented in Section 5.
 557 All hyperparameters and architectural choices are specified within these sections, and we will make
 558 the source code, training scripts, and trained models publicly available upon acceptance to facilitate
 559 full verification of our results.
 560

561
562
REFERENCES

563 Structural topology optimisation based on a multi-agent model. <https://www.sciencedirect.com/science/article/pii/S0141029623013937>, 2023.
 564 Engineering Structures, Elsevier. Accessed 2025-08-26.
 565

566 Brandon Ayal a. Topology-driven performance analyses in consensus algorithms for multi-agent
 567 systems. Master’s thesis, University of Texas at Arlington, Arlington, TX, 2025. URL https://mavmatrix.uta.edu/mechaerospace_theses/1030/.
 568

569 Guangyao Chen et al. Autoagents: A framework for automatic agent generation. *arXiv:2309.17288*,
 570 2023a. URL <https://arxiv.org/abs/2309.17288>.
 571

572 Wenhui Chen et al. Agentverse: Facilitating multi-agent collaboration and exploring emergent be-
 573 haviors. *arXiv:2308.10848*, 2023b. URL <https://arxiv.org/abs/2308.10848>.
 574

575 Yao Chen, Jinhu Lü, Xinghuo Yu, and David J. Hill. Multi-agent systems with dynamical topologies:
 576 Consensus and applications. *IEEE Circuits and Systems Magazine*, 13(3):21–34, 2013. doi:
 577 10.1109/MCAS.2013.2271443.
 578

579 Dhrubajit Chowdhury and Hassan K. Khalil. Fast consensus in multi-agent systems with star topol-
 580 ogy using high gain observers. *IEEE Control Systems Letters*, 1(1):188–193, 2017.
 581

582 Shifei Ding, Wei Du, Ling Ding, Lili Guo, and Jian Zhang. Learning efficient and robust multi-
 583 agent communication via graph information bottleneck. In *AAAI*, volume 38, pp. 17346–
 584 17353, 2024. doi: 10.1609/aaai.v38i16.29682. URL <https://doi.org/10.1609/aaai.v38i16.29682>.
 585

586 Wei Du, Shifei Ding, Lili Guo, Jian Zhang, and Ling Ding. Expressive multi-agent communication
 587 via identity-aware learning. In *AAAI*, volume 38, pp. 17354–17361, 2024. doi: 10.1609/aaai.
 588 v38i16.29683. URL <https://doi.org/10.1609/aaai.v38i16.29683>.
 589

590 Yilun Du et al. Improving factuality and reasoning in language models through multiagent debate.
 591 *arXiv:2305.14325*, 2023. URL <https://arxiv.org/abs/2305.14325>.
 592

593 Yao Fu et al. Complexity-based prompting for multi-step reasoning. *arXiv:2210.00720*, 2022. URL
<https://arxiv.org/abs/2210.00720>.

594 Ning Gong, Michael Korostelev, Qiangguo Ren, Li Bai, Saroj Biswas, and Frank Ferrese.
 595 Fault tolerant (n, k)-star power network topology for multi-agent communication in auto-
 596 mated power distribution systems. <https://d1wqtxts1xzle7.cloudfront.net/80670305/pdf-libre.pdf>, 2015. Proceedings/Journal venue not clearly specified; accessed 2025-08-26.

599 Aaron Helsinger, Michael Thome, and Todd Wright. Cougaar: A scalable, distributed multi-agent
 600 architecture. In *Proceedings of the IEEE International Conference on Systems, Man and Cyber-
 601 netics (SMC)*, pp. 1910–1917, The Hague, Netherlands, 2004.

603 Jonathan Ho and Tim Salimans. Classifier-free diffusion guidance. *arXiv:2207.12598*, 2021.

604 Jonathan Ho, Ajay Jain, and Pieter Abbeel. Denoising diffusion probabilistic models. In *NeurIPS*,
 605 2020.

607 Sirui Hong et al. MetaGPT: Meta programming for multi-agent collaborative framework.
 608 *arXiv:2308.00352*, 2023.

609 Shengchao Hu, Li Shen, Ya Zhang, and Dacheng Tao. Learning multi-agent communication
 610 from graph modeling perspective. In *ICLR*, 2024a. URL <https://doi.org/10.48550/arXiv.2405.08550>.

613 Shunyu Hu et al. Automated design of agentic systems. *arXiv:2408.08435*, 2024b. URL <https://arxiv.org/abs/2408.08435>.

615 Mengda Ji, Genjiu Xu, and Liying Wang. Cora: Coalitional rational advantage decomposition
 616 for multi-agent policy gradients. *arXiv:2506.04265*, 2025. URL <https://doi.org/10.48550/arXiv.2506.04265>.

618 Dongfu Jiang, Bill Yuchen Lin, and Xiang Ren. LLM-Blender: Ensembling large language models
 619 with pairwise ranking and generative fusion. In *ACL*, 2023. URL <https://aclanthology.org/2023.acl-long.792/>.

622 Guohao Li et al. CAMEL: Communicative agents for “mind” exploration with language models.
 623 *arXiv:2303.17760*, 2023.

624 Xinran Li, Xiaolu Wang, Chenjia Bai, and Jun Zhang. Exponential topology-enabled scalable com-
 625 munication in multi-agent reinforcement learning. In *ICLR*, 2025. URL <https://arxiv.org/abs/2502.19717>.

628 Sijia Liu et al. Zeroth-order stochastic gradient methods for nonconvex optimization. In *NeurIPS*,
 629 2018.

636 Zhen Liu et al. A dynamic llm-powered agent network for task-oriented collaboration.
 631 *arXiv:2310.02170*, 2023. URL <https://arxiv.org/abs/2310.02170>.

633 Yat Long Lo, Biswa Sengupta, Jakob Foerster, and Michael Noukhovitch. Learning multi-agent
 634 communication with contrastive learning. *arXiv:2307.01403*, 2024. URL <https://arxiv.org/abs/2307.01403>.

636 Manuel Madeira, Clement Vignac, Dorina Thanou, and Pascal Frossard. Generative modelling of
 637 structurally constrained graphs. In *NeurIPS*, 2024. URL <https://arxiv.org/abs/2406.17341>.

639 Yurii Nesterov and Vladimir Spokoiny. Random gradient-free minimization of convex functions.
 640 *Foundations of Computational Mathematics*, 2017.

642 Long Ouyang et al. Training language models to follow instructions with human feedback.
 643 *arXiv:2203.02155*, 2022.

644 Chen Qian et al. Scaling large-language-model-based multi-agent collaboration. *arXiv:2406.07155*,
 645 2024. URL <https://arxiv.org/abs/2406.07155>.

647 Yu Shang et al. Agentsquare: Automatic llm agent search in modular design space.
 648 *arXiv:2410.06153*, 2024. URL <https://arxiv.org/abs/2410.06153>.

648 Yang Song and Stefano Ermon. Score-based generative modeling through stochastic differential
 649 equations. In *ICLR*, 2021.

650

651 Qi Sun, Junyi Li, Zijun Yao, Shoujin Wang, Philip S. Yu, and Wenjie Zhang. Assemble your crew:
 652 Automatic multi-agent communication topology design via autoregressive graph generation.
 653 *arXiv preprint arXiv:2507.18224*, 2025. URL <https://arxiv.org/abs/2507.18224>.

654 Clement Vignac et al. DiGress: A generative model for graphs via diffusion. In *NeurIPS*, 2023.

655

656 Xuezhi Wang et al. Self-consistency improves chain of thought reasoning in language models. In
 657 *ICLR*, 2023a. URL <https://arxiv.org/abs/2203.11171>.

658 Zhen Wang et al. Unleashing the emergent cognitive synergy of llms: A multi-persona self-
 659 collaboration framework. *arXiv:2307.05300*, 2023b. URL <https://arxiv.org/abs/2307.05300>.

660

661 Jason Wei et al. Chain-of-thought prompting elicits reasoning in large language models.
 662 *arXiv:2201.11903*, 2022. URL <https://arxiv.org/abs/2201.11903>.

663

664 Zhenzhong Wu et al. AutoGen: Enabling next-gen LLM applications via multi-agent conversation.
 665 *arXiv:2308.08155*, 2023.

666

667 Dan Xiao and Ah-Hwee Tan. Cooperative reinforcement learning in topology-based multi-agent
 668 systems. *Autonomous Agents and Multi-Agent Systems*, 26(1):86–119, 2013. doi: 10.1007/
 669 s10458-011-9183-4.

670

671 Zhe Xu, Ruizhong Qiu, Yuzhong Chen, Huiyuan Chen, Xiran Fan, Menghai Pan, Zhichen Zeng,
 672 Mahashweta Das, and Hanghang Tong. Discrete-state continuous-time diffusion for graph gener-
 673 ation, 2024. URL <https://arxiv.org/abs/2405.11416>.

674

675 Shijie Yang, Yihao Feng, Junning Song, Peijie Sun, Yili Wang, Chen Li, Wenjie Zhang, Shirui Pan,
 676 and Chengqi Zhang. Anymac: Cascading flexible multi-agent collaboration via next-agent pre-
 677 diction. *arXiv preprint arXiv:2506.17784*, 2025. URL <https://arxiv.org/abs/2506.17784>.

678

679 Jiaxuan You, Bowen Liu, Rex Ying, Vijay Pande, and Jure Leskovec. Graph convolutional policy
 680 network for goal-directed molecular graph generation. In *NeurIPS*, 2018. URL <https://doi.org/10.48550/arXiv.1806.02473>.

681

682 Tingting Yuan, Hwei-Ming Chung, Jie Yuan, and Xiaoming Fu. Dacom: Learning delay-aware com-
 683 munication for multi-agent reinforcement learning. In *AAAI*, 2023. URL <https://arxiv.org/abs/2212.01619>.

684

685 Guibin Zhang, Yanwei Yue, Zhixun Li, Sukwon Yun, Guancheng Wan, Kun Wang, Dawei Cheng,
 686 Jeffrey Xu Yu, and Tianlong Chen. Cut the crap: An economical communication pipeline for llm-
 687 based multi-agent systems. *arXiv preprint arXiv:2410.02506*, 2024. doi: 10.48550/arXiv.2410.
 688 02506. URL <https://arxiv.org/abs/2410.02506>. ICLR 2025 (poster), OpenReview
 689 version available.

690

691 Guibin Zhang, Yanwei Yue, Xiangguo Sun, Guancheng Wan, Miao Yu, Junfeng Fang, Kun
 692 Wang, Tianlong Chen, and Dawei Cheng. G-designer: Architecting multi-agent communi-
 693 cation topologies via graph neural networks. *arXiv preprint arXiv:2410.11782*, 2025a. doi:
 694 10.48550/arXiv.2410.11782. URL <https://arxiv.org/abs/2410.11782>.

695

696 Guibin Zhang et al. Multi-agent architecture search via agentic supernet. *arXiv:2502.04180*, 2025b.
 697 URL <https://arxiv.org/abs/2502.04180>.

698

699 Guochen Zhang, Aolong Zhang, Chaoli Sun, and Qing Ye. An evolutionary algorithm for multi-
 700 objective workflow scheduling with adaptive dynamic grouping. *Electronics*, 14(13):2586, 2025c.
 701 doi: 10.3390/electronics14132586. URL <https://www.mdpi.com/2079-9292/14/13/2586>.

702

703 Jiaxin Zhang et al. Aflow: Automating agentic workflow generation. In *ICLR*, 2025d. URL <https://arxiv.org/abs/2410.10762>.

702 Lingxiao Zhao, Xueying Ding, and Leman Akoglu. Pard: Permutation-invariant autoregressive
703 diffusion for graph generation. In *NeurIPS*, 2024. URL [https://doi.org/10.48550/
704 arXiv.2402.03687](https://doi.org/10.48550/arXiv.2402.03687).

705 Han Zhou, Xingchen Wan, Ruoxi Sun, Hamid Palangi, Shariq Iqbal, Ivan Vulić, Anna Korhonen,
706 and Sercan Ö. Arik. Multi-agent design: Optimizing agents with better prompts and topologies.
707 *arXiv preprint arXiv:2502.02533*, 2025. URL <https://arxiv.org/abs/2502.02533>.

708 Changxi Zhu, Mehdi Dastani, and Shihan Wang. Reducing variance caused by communication in
709 decentralized multi-agent deep reinforcement learning, 2025. URL [https://arxiv.org/
710 abs/2502.06261](https://arxiv.org/abs/2502.06261).

711 Qiuming Zhu. The topologies of cooperation in knowledge intensive multi-agent systems.
712 In *Proceedings of the IEEE International Conference on Systems, Man and Cybernetics (SMC)*, 2003.
713 URL [https://ieeexplore.ieee.org/abstract/document/
714 1245130](https://ieeexplore.ieee.org/abstract/document/1245130). IEEE Xplore abstract #1245130.

715 Qiuming Zhu. Topologies of agents interactions in knowledge intensive multi-agent systems
716 for networked information services. *Advanced Engineering Informatics*, 20(1):31–45, 2006.
717 doi: 10.1016/j.aei.2005.08.001. URL [https://www.sciencedirect.com/science/
718 article/pii/S1474034605000728](https://www.sciencedirect.com/science/article/pii/S1474034605000728).

719 Mingchen Zhuge et al. Language agents as optimizable graphs. *arXiv:2402.16823*, 2024. URL
720 <https://arxiv.org/abs/2402.16823>.

721

722

723

724

725

726

727

728

729

730

731

732

733

734

735

736

737

738

739

740

741

742

743

744

745

746

747

748

749

750

751

752

753

754

755

756 **A ALGORITHM**
757758 **Algorithm 1** Guided Topology Diffusion (GTD) Generation
759

760 1: **Input:** Task condition C_{new} , trained models $\mathcal{G}_{\theta^*}, \mathcal{P}_{\phi^*}$, weights w_u, w_c .
761 2: Sample $A_T \sim \mathcal{N}(0, \mathbf{I})$.
762 3: **for** $t = T, \dots, 1$ **do**
763 4: Predict the unguided clean graph: $\hat{A}_0^{(t)} = \mathcal{G}_{\theta^*}(A_t, C_{\text{new}}, t)$.
764 5: Generate K candidates: $\{A_{0,k}^{(t)}\}_{k=1}^K$, where $A_{0,k}^{(t)} \sim \text{Bernoulli}(\text{sigmoid}(\hat{A}_0^{(t)}))$.
765 6: Evaluate candidates: For $k = 1 \dots K$, compute $[\hat{u}_k, \hat{c}_k]^T = \mathcal{P}_{\phi^*}(A_{0,k}^{(t)}, C_{\text{new}})$.
766 7: Select best candidate via ZO: $A_{0,\text{best}}^{(t)} = \arg \max_{A_{0,k}^{(t)}} (w_u \cdot \hat{u}_k - w_c \cdot \hat{c}_k)$.
767 8: Compute posterior mean μ_{post} and variance Σ_{post} for $q(A_{t-1}|A_t, A_{0,\text{best}}^{(t)})$.
768 9: Sample the next state: $A_{t-1} \sim \mathcal{N}(\mu_{\text{post}}, \Sigma_{\text{post}})$.
769 10: **end for**
770 11: **Output:** The final graph A_0 .

773 **B DATA STATISTICS**
774776 We conclude the data statistics in the table 2.
777778 Table 2: Dataset descriptions and statistics.
779

Category	Dataset	Answer Type	Metric	#Test	License
General reasoning	MMLU	Multi-choice	Acc.	1,530	MIT License
	GSM8K	Number	Acc.	1,319	MIT License
	MultiArith	Number	Acc.	180	Unspecified
	SVAMP	Number	Acc.	300	MIT License
Math reasoning	Math	Number	Acc.	500	MIT License
	HumanEval	Code	Pass@1	164	MIT License

788 **C THEORETICAL JUSTIFICATION**
789791 In this section, we provide a more formal theoretical underpinning for the GTD framework. We
792 begin by framing the graph diffusion model within the lens of variational inference and then analyze
793 the convergence properties of our proxy-guided synthesis process.
794795 **C.1 VARIATIONAL PERSPECTIVE OF GRAPH DIFFUSION**
796797 The generative process of denoising diffusion models can be rigorously justified as a procedure for
798 optimizing the Evidence Lower Bound (ELBO) of the data's log-likelihood.
799800 **Definition C.1** (Evidence Lower Bound (ELBO)). *Given a data point A_0 , a joint distribution
801 $p_{\theta}(A_{0:T}|C)$, and a variational posterior $q(A_{1:T}|A_0)$, the ELBO for the conditional log-likelihood
802 $\log p_{\theta}(A_0|C)$ is defined as:*

803
$$\mathcal{L}_{\text{ELBO}} = \mathbb{E}_{q(A_{1:T}|A_0)} \left[\log \frac{p_{\theta}(A_{0:T}|C)}{q(A_{1:T}|A_0)} \right] \leq \log p_{\theta}(A_0|C) \quad (10)$$

805 This lower bound can be decomposed into a series of terms that are more amenable to optimization:
806

807
$$\begin{aligned} \mathcal{L}_{\text{ELBO}} &= \mathbb{E}_q [\log p_{\theta}(A_0|A_1, C)] - D_{KL}(q(A_T|A_0)||p(A_T)) \\ &\quad - \sum_{t=2}^T D_{KL}(q(A_{t-1}|A_t, A_0)||p_{\theta}(A_{t-1}|A_t, C)) \end{aligned} \quad (11)$$

810 Optimizing the ELBO involves minimizing the KL-divergence between the true posterior of the
 811 forward process and the learned reverse process. The forward process posterior is known to be
 812 tractable.

813 **Lemma C.2** (Forward Process Posterior). *The posterior distribution $q(A_{t-1}|A_t, A_0)$ is a Gaussian
 814 distribution given by:*

$$816 \quad q(A_{t-1}|A_t, A_0) = \mathcal{N}\left(A_{t-1}; \tilde{\mu}_t(A_t, A_0), \tilde{\beta}_t \mathbf{I}\right) \quad (12)$$

817 where $\tilde{\mu}_t(A_t, A_0) = \frac{\sqrt{\bar{\alpha}_{t-1}}\beta_t}{1-\bar{\alpha}_t}A_0 + \frac{\sqrt{\alpha_t}(1-\bar{\alpha}_{t-1})}{1-\bar{\alpha}_t}A_t$ and $\tilde{\beta}_t = \frac{1-\bar{\alpha}_{t-1}}{1-\bar{\alpha}_t}\beta_t$.

821 By parameterizing the reverse process $p_\theta(A_{t-1}|A_t, C)$ as a Gaussian whose mean is predicted by
 822 a neural network, we can connect the variational objective to a simpler, more practical training
 823 objective.

824 **Theorem C.3** (Optimality of the Denoising Objective). *Assuming the reverse process $p_\theta(A_{t-1}|A_t, C)$ is Gaussian, minimizing the KL-divergence term
 825 $D_{KL}(q(A_{t-1}|A_t, A_0)||p_\theta(A_{t-1}|A_t, C))$ in Eq. 11 with respect to θ is equivalent to training
 826 a denoising network $\mathcal{G}_\theta(A_t, C, t)$ to predict A_0 from A_t by minimizing the L2 loss:*

$$828 \quad \mathcal{L}_{\text{simple}} = \mathbb{E}_{t, A_0, C, \epsilon} \left[\|A_0 - \mathcal{G}_\theta(\sqrt{\bar{\alpha}_t}A_0 + \sqrt{1-\bar{\alpha}_t}\epsilon, C, t)\|^2 \right] \quad (13)$$

831 *Proof.* Our goal is to minimize the KL divergence between the true posterior and the learned reverse
 832 process:

$$834 \quad L_t = D_{KL}(q(A_{t-1}|A_t, A_0)||p_\theta(A_{t-1}|A_t, C)) \quad (14)$$

836 Both distributions are Gaussian: $q(A_{t-1}|A_t, A_0) = \mathcal{N}(\cdot; \tilde{\mu}_t(A_t, A_0), \tilde{\beta}_t \mathbf{I})$ and $p_\theta(A_{t-1}|A_t, C) =$
 837 $\mathcal{N}(\cdot; \mu_\theta(A_t, C, t), \sigma_t^2 \mathbf{I})$. For simplicity, we fix the variance of the reverse process to match the
 838 true posterior, $\sigma_t^2 = \tilde{\beta}_t$. The KL divergence between two multivariate Gaussians $\mathcal{N}(\mu_1, \Sigma_1)$ and
 839 $\mathcal{N}(\mu_2, \Sigma_2)$ simplifies when $\Sigma_1 = \Sigma_2 = \sigma^2 \mathbf{I}$ to $\frac{1}{2\sigma^2} \|\mu_1 - \mu_2\|^2$. Therefore, minimizing the KL
 840 divergence is equivalent to minimizing the squared Euclidean distance between their means:

$$841 \quad L_t = \mathbb{E}_{A_0, C, \epsilon} \left[\frac{1}{2\tilde{\beta}_t} \|\tilde{\mu}_t(A_t, A_0) - \mu_\theta(A_t, C, t)\|^2 \right] \quad (15)$$

844 The expression for the true posterior mean is $\tilde{\mu}_t(A_t, A_0) = \frac{\sqrt{\bar{\alpha}_{t-1}}\beta_t}{1-\bar{\alpha}_t}A_0 + \frac{\sqrt{\alpha_t}(1-\bar{\alpha}_{t-1})}{1-\bar{\alpha}_t}A_t$. We
 845 parameterize our model's mean μ_θ to have the same functional form, but predicting A_0 with our
 846 network $\mathcal{G}_\theta(A_t, C, t)$:

$$848 \quad \mu_\theta(A_t, C, t) = \frac{\sqrt{\bar{\alpha}_{t-1}}\beta_t}{1-\bar{\alpha}_t} \mathcal{G}_\theta(A_t, C, t) + \frac{\sqrt{\alpha_t}(1-\bar{\alpha}_{t-1})}{1-\bar{\alpha}_t} A_t \quad (16)$$

851 Substituting this into the loss function, the terms involving A_t cancel out:

$$853 \quad L_t = \mathbb{E}_{A_0, C, \epsilon} \left[\frac{1}{2\tilde{\beta}_t} \left\| \frac{\sqrt{\bar{\alpha}_{t-1}}\beta_t}{1-\bar{\alpha}_t} A_0 - \frac{\sqrt{\bar{\alpha}_{t-1}}\beta_t}{1-\bar{\alpha}_t} \mathcal{G}_\theta(A_t, C, t) \right\|^2 \right] \quad (17)$$

$$855 \quad = \mathbb{E}_{A_0, C, \epsilon} \left[\frac{(\sqrt{\bar{\alpha}_{t-1}}\beta_t)^2}{2\tilde{\beta}_t(1-\bar{\alpha}_t)^2} \|A_0 - \mathcal{G}_\theta(A_t, C, t)\|^2 \right] \quad (18)$$

858 Since the term outside the norm is a positive constant for a given timestep t , minimizing L_t with
 859 respect to θ is equivalent to minimizing the simpler objective:

$$861 \quad \mathcal{L}'_t = \mathbb{E}_{A_0, C, \epsilon} [\|A_0 - \mathcal{G}_\theta(A_t, C, t)\|^2] \quad (19)$$

863 By substituting $A_t = \sqrt{\bar{\alpha}_t}A_0 + \sqrt{1-\bar{\alpha}_t}\epsilon$ and taking the expectation over all timesteps t , we arrive
 864 at the simplified loss function $\mathcal{L}_{\text{simple}}$ stated in the theorem. \square

864 C.2 ANALYSIS OF PROXY-GUIDED SYNTHESIS
865866 We now analyze the role of the surrogate model and the ZO optimization step in guiding the synthesis
867 towards high-reward topologies.868 **Definition C.4** (ϵ -Accurate Surrogate Model). *A surrogate reward model \mathcal{P}_ϕ is ϵ_{\max} -accurate with
869 respect to a true reward function $R(A, C)$ if, for any valid topology A and condition C , the approx-
870 imation error is bounded:*

871
$$|R(A, C) - \mathcal{P}_\phi(A, C)| \leq \epsilon_{\max} \quad (20)$$

872

873 The accuracy of this model directly bounds the sub-optimality of the topology generated by an ideal
874 proxy-guided optimizer.875 **Theorem C.5** (Performance Gap Bound). *Let $A^* = \arg \max_A R(A, C)$ be the true optimal topol-
876 ogy and $A_{\text{proxy}}^* = \arg \max_A \mathcal{P}_\phi(A, C)$ be the topology found by an ideal optimizer using an ϵ_{\max} -
877 accurate proxy. The performance gap is bounded by:*

878
$$R(A^*, C) - R(A_{\text{proxy}}^*, C) \leq 2\epsilon_{\max} \quad (21)$$

879

880 *Proof.* By definition of A_{proxy}^* as the maximizer of the proxy reward function, we have
881 $\mathcal{P}_\phi(A_{\text{proxy}}^*, C) \geq \mathcal{P}_\phi(A^*, C)$. From the definition of an ϵ_{\max} -accurate surrogate model, we know
882 that for any topology A , $R(A, C) \geq \mathcal{P}_\phi(A, C) - \epsilon_{\max}$. Applying this bound to A_{proxy}^* , we get:

883
$$R(A_{\text{proxy}}^*, C) \geq \mathcal{P}_\phi(A_{\text{proxy}}^*, C) - \epsilon_{\max} \quad (22)$$

884 Combining this with the optimality condition of A_{proxy}^* gives:

885
$$R(A_{\text{proxy}}^*, C) \geq \mathcal{P}_\phi(A^*, C) - \epsilon_{\max} \quad (23)$$

886 Again, from the ϵ_{\max} -accuracy definition applied to A^* , we can state that $\mathcal{P}_\phi(A^*, C) \geq R(A^*, C) -$
887 ϵ_{\max} . Substituting this into the previous inequality yields:

888
$$R(A_{\text{proxy}}^*, C) \geq (R(A^*, C) - \epsilon_{\max}) - \epsilon_{\max} \quad (24)$$

889
$$= R(A^*, C) - 2\epsilon_{\max} \quad (25)$$

890 Rearranging this final expression gives the desired bound:

891
$$R(A^*, C) - R(A_{\text{proxy}}^*, C) \leq 2\epsilon_{\max} \quad (26)$$

892 This completes the proof. \square
893894 **Corollary C.6** (Perfect Surrogate). *If the surrogate model is perfect, i.e., $\epsilon_{\max} = 0$, then any topol-
895 ogy A_{proxy}^* that maximizes the proxy reward also maximizes the true reward, yielding $R(A_{\text{proxy}}^*, C) =$
896 $R(A^*, C)$.*897 **Definition C.7** (ZO-Guided Denoising Step). *At a diffusion step t , given the unguided prediction
898 $\hat{A}_0^{(t)} = \mathcal{G}_{\theta^*}(A_t, C, t)$, the ZO-guided denoising step replaces $\hat{A}_0^{(t)}$ with $A_{0,\text{best}}^{(t)}$, where:*

899
$$A_{0,\text{best}}^{(t)} = \arg \max_{A \in \{A_{0,k}^{(t)}\}_{k=1}^K} \mathcal{P}_\phi(A, C) \quad (27)$$

900 and each candidate $A_{0,k}^{(t)}$ is a discrete sample drawn from a distribution parameterized by $\hat{A}_0^{(t)}$, e.g.,
901 $A_{0,k}^{(t)} \sim \text{Bernoulli}(\sigma(\hat{A}_0^{(t)}))$.902 This ZO step can be viewed as approximating a gradient ascent step on the proxy reward land-
903 scape. Let $J(\hat{A}_0) = \mathbb{E}_{A \sim p(A|\hat{A}_0)}[\mathcal{P}_\phi(A, C)]$. The true gradient $\nabla_{\hat{A}_0} J$ is intractable. The ZO step
904 provides an update direction, $\Delta_t = A_{0,\text{best}}^{(t)} - \hat{A}_0^{(t)}$, which serves as a stochastic estimate of the as-
905 cent direction. The use of multiple samples ($K > 1$) reduces the variance of this estimate. The
906 guided update for the next state A_{t-1} is then computed using the posterior conditioned on $A_{0,\text{best}}^{(t)}$
907 instead of $\hat{A}_0^{(t)}$, effectively biasing the sampling trajectory towards regions of higher proxy reward.
908 This greedy, step-wise maximization provides a computationally efficient method for incorporating
909 non-differentiable objectives directly into the generative process.

918 D SUPPLEMENTARY RESULTS: SCALABILITY ANALYSIS
919920 To assess the scalability of GTD for larger multi-agent systems, we measured the GPU memory
921 consumption of the diffusion generator and proxy model as the number of agents (N) increases. As
922 shown in Table 3, the memory requirement scales linearly and remains well within the capacity of
923 standard consumer hardware even for large swarms.
924925 Table 3: The GPU cost with increasing number of agents.
926927

#Agents	5	50	100	1000
Memory (GB)	2.8	3.4	3.9	4.9

928929 This confirms that while our current benchmarks focus on small-team reasoning (4-5 agents), the
930 GTD framework is technically capable of optimizing large-scale agent organizations without hitting
931 hardware bottlenecks.
932933 E SUPPLEMENTARY RESULTS: GENERALIZATION TO OPEN-SOURCE
934 MODELS AND HARDER BENCHMARKS
935936 To verify that our gains are not specific to the GPT-4o-mini backbone, we extended our experiments
937 to the open-source **Qwen-3-8B** model on GSM8K. GTD achieved **93.1%** accuracy, outperforming
938 both the base model (87.8%) and the MaAS baseline (91.8%). Furthermore, we evaluated GTD
939 on the challenging **LiveCodeBench** (Pass@1). GTD achieved **30.8%**, surpassing the Base Model
940 (25.4%) and MaAS (29.3%), demonstrating that our topology optimization provides consistent ben-
941 efits across different model families and task difficulties.
942943 F COMPUTATIONAL RESOURCES
944945 All experiments, including the training of the surrogate and diffusion models, as well as the multi-
946 agent system simulations for data generation and evaluation, were conducted on a server equipped
947 with four NVIDIA A6000 GPUs, each with 48GB of VRAM.
948949 G ETHICS AND SOCIETAL IMPACT
950951 This research is focused on improving the efficiency and effectiveness of multi-agent systems
952 (MAS), which can lead to positive societal impacts like accelerating scientific discovery and reduc-
953 ing the energy consumption of large-scale AI computations. However, we recognize that a frame-
954 work for optimizing agent coordination is a dual-use technology. In the wrong hands, it could po-
955 tentially be used to orchestrate malicious activities, such as coordinating disinformation campaigns
956 or automated attacks. Furthermore, the performance of our system is dependent on the initial dataset
957 used to train our models; any biases present in this data could lead to the generation of suboptimal or
958 inequitable communication structures for certain tasks. Our work is intended purely for beneficial
959 applications, and we advocate for the establishment of strong ethical guidelines and safeguards in
960 the development of advanced agentic systems.
961962 H THE USE OF LARGE LANGUAGE MODELS (LLMs)
963964 Large Language Models (LLMs) are a central component of our research methodology. The multi-
965 agent systems evaluated in this paper are composed of agents powered by GPT-4o-mini, which
966 perform the reasoning and communication necessary to solve complex tasks. The performance of
967 these LLM agents is fundamental to generating our training data and evaluating the effectiveness of
968 the communication topologies created by our GTD framework.
969970 Separately, for the preparation of this manuscript, our use of LLMs was strictly limited to polishing
971 the language and generating figures. All underlying research and intellectual content, including the

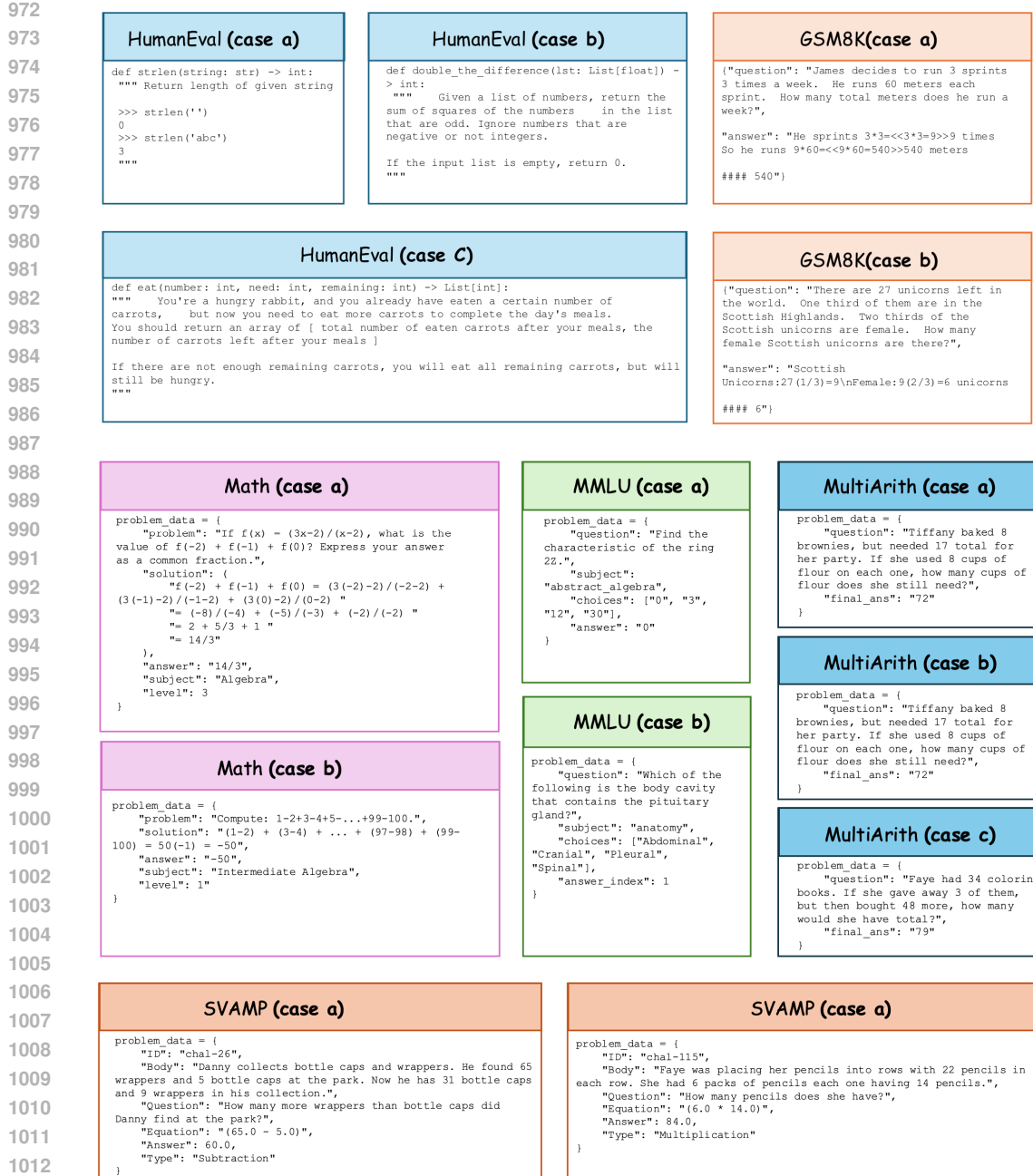


Figure 8: Case study of the communication topologies designed by GTD on all benchmarks.

GTD framework, its theoretical foundations, experimental design, and the analysis of results, was completed entirely by the authors.

I PROMPTS

Figure 8 presents the topologies designed by GTD under varying query difficulties for all the benchmarks.

1026 J AGENT ROLES AND DESCRIPTIONS

1028 Figure 9 visualizes a set of specialized agents. These roles provide diverse perspectives that are
 1029 combined to produce the final answer.

 Knowlegable Expert You are a knowlegable expert in question answering. Please give several key entities that need to be searched in wikipedia to solve the problem, for example: catfish effect, broken window effect, Shakespeare. If there is no entity in the question that needs to be searched in Wikipedia, you don't have to provide it	 Wiki Researcher You will be given a question and a wikipedia overview of the key entities within it. Please refer to them step by step to give your answer. And point out potential issues in other agent's analysis.	 Critic You are an excellent critic. Please point out potential issues in other agent's analysis point by point.
 Psychologist You are a psychologist. You are good at psychology, sociology, and philosophy. You give people scientific suggestions that will make them feel better.	 Historian You research and analyze cultural, economic, political, and social events in the past, collect data from primary sources and use it to develop theories about what happened during various periods of history.	 Economist You are good at economics, finance, and business. You have experience on understanding charts while interpreting the macroeconomic environment prevailing across world economies.
 Doctor You are a doctor and come up with creative treatments for illnesses or diseases. You are able to recommend conventional medicines, herbal remedies and other natural alternatives. You also consider the patient's age, lifestyle and medical history when providing your recommendations.	 Programmer You are good at computer science, engineering, and physics. You have experience in designing and developing computer software and hardware.	 Fake You are a liar who only tell lies.
		 Lawyer You are good at law, politics, and history.

1051 Figure 9: Overview of the different roles in our multi-agent question answering framework. Each role represents a distinct perspective or expertise (e.g., knowledge extraction, searching, critique, mathematics, psychology, history, medicine, economics, programming, law, or deliberate deception).